Neutron Star Astrophysics at the Crossroads: Magnetars and the Multimessenger Revolution
Proceedings IAU Symposium No. 363, 2023
E. Troja & M. G. Baring, eds.
doi:10.1017/S1743921322001144

Neutron Star Equation of State Constraints from *NICER* and Multimessenger Gravitational Wave Observations

Geert Raaijmakers

GRAPPA, University of Amsterdam, Amsterdam, the Netherlands
email: g.raaijmakers@uva.nl

Abstract. The dense matter equation of state (EoS), describing the state of matter under the extreme conditions found in neutron stars, is not accurately known. However, significant process has been made in recent years through the emergence of new observational avenues of neutron stars. Firstly, the X-ray timing telescope *NICER* has delivered two joint mass-radius measurements, for pulsars PSR J0030+0451 and PSR J0740+6620, using pulse profile modeling. Secondly, gravitational wave detections of binary neutron star (BNS) mergers allow for a measurement of the EoS-dependent tidal deformability, as demonstrated in the first detected BNS merger GW170817. Additionally, electromagnetic radiation from the subsequent ultraviolet-optical-infrared transient (the kilonova) originating from the ejected material in GW170817 further probes the binary system and the EoS. We demonstrate how the joint analysis of these multi-messenger observations of neutron stars significantly constrains the dense matter EoS. We then describe, in more detail, a framework to jointly analyse a gravitational wave signal and the accompanying kilonova light curves, focusing on possible future black hole–neutron star (BHNS) mergers. We highlight the potential for multimessenger BHNS to constrain the tidal deformability of the neutron star, thereby increasing our understanding of the dense matter EoS.

Keywords. Neutron Stars, Dense matter, Gravitational Waves, Kilonova

1. Introduction

The core of neutron stars give a unique insight in dense matter physics due to the extreme pressure particles are subjected to, something we are currently not able to recreate in terrestrial experiments. For matter at these high densities, up to a few times nuclear saturation density (n_0), many theoretical models exist that predict different kinds of states such particles can be in, ranging from extremely neutron-rich nucleonic matter, to phase transitions to stable quark matter or hyperons or a color superconducting phase (see, e.g., Baym et al. (2018) for a review).

Information on the state of dense matter is encoded in the equation of state (EoS) of neutron stars. Although the exact EoS is still unknown, a lot of progress has been made in recent years. An important contribution for these advancements came from the first mass-radius measurements from the *Neutron star Interior Composition Explorer* (*NICER*). As an X-ray timing instrument on board the *International Space Station*, *NICER* employs pulse profile modeling to jointly constrain the mass and radius of rotation-powered millisecond pulsars. This technique makes use of the strong gravitational field around the neutron star affecting the X-ray photons emitted from the surface to infer the compactness of the star. So far, *NICER* has published the first results of two pulsars, PSR

J0030+0451 (Miller et al. (2019), Riley et al. (2019)) and PSR J0470+6620 (Miller et al. (2021), Riley et al. (2021)).

Novel constraints on the EoS were also possible due to the first ever detection of gravitational waves (GW) coming from the binary neutron star (BNS) merger GW170817 (Abbott et al. (2017)). The authors in Abbott et al. (2018) measured the dephasing in the GW signal, due to matter effects of the two neutron stars, to constrain their tidal deformability, a parameter that is intrinsically coupled to the EoS. GW170817 was also the first multimessenger GW event, as a counterpart was detected across the electromagnetic (EM) spectrum following the merger. One of the EM counterparts was an ultraviolet/optical/infrared (UVOIR) transient, commonly referred to in the literature as a kilonova. The kilonova is thought to be powered by radioactive decay of heavy elements formed in the neutron-rich material that is ejected during and after the violent merger (Li & Paczyinski (1998); Metzger (2019)). The amount of material that is ejected, and as a result the properties of the observed light curve, depend crucially on the tidal deformability of the neutron stars, thereby providing further constraints on the EoS (see, e.g., Krüger & Foucart (2020)).

In this proceeding I will review the current constraints we have on the dense matter EoS from joint analyses of *NICER* measurements, radio mass measurements, and (multimessenger) GW events, as well as give an outlook on how multimessenger black hole - neutron star (BHNS) mergers may provide additional stringent constraints.

2. Dense Matter EoS Constraints from Multimessenger Observations

There have been many recent papers constraining the dense matter EoS with some combination of *NICER* observations, gravitational wave observations and low-density nuclear information. Three of the most commonly used methods to do so are i); parametric EoS inference, ii); non-parametric EoS inference, iii); and discrete EoS inference. The latter pre-computes a large sample of EoS which are subsequently discretely sampled during parameter estimation (see, e.g., Capano et al. (2020); Pang et al. (2021)). In the case of non-parametric EoS inference, the EoS is commonly modeled using Gaussian Processes to allow for any functional form (see, e.g., Landry & Essick (2019); Essick et al. (2020); Legred et al. (2021)). For parametric EoS inference, the EoS is parameterized by a fixed functional form, such as piecewise-polytropes (Read et al. (2009); Hebeler et al. (2013)), spectral representations (Lindblom (2010)) or functions based on the speed of sound in the neutron star (Greif et al. (2019)). In the following I will review constraints set on the EoS by different observations, using Bayesian parameter estimation with a piecewise-polytropic parameterization. At lower densities, below $1.1n_0$, the EoS parameterization is bounded by calculations of neutron matter through the modeling of nucleon-nucleon and three-nucleon interactions within a chiral effective field theory framework (Hebeler et al. (2013)).

2.1. *Radio mass measurements of massive pulsars*

Currently, a large part of the constraining power comes from mass measurements of massive pulsars. In the context of the dense matter EoS, the most interesting measurements are enabled by accurately determining the Shapiro-delay of pulsars in binaries with pulsar timing. This method has delivered a precise measurement of the most massive pulsar known to date, PSR J0740+6620 (Cromartie et al. (2020); Fonseca et al. (2021)), with a mass of 2.08 ± 0.07 $M_\odot$. The upper left panel of 1 shows the constraints on the EoS from this measurement when assuming a piecewise-polytropic parameterization. Here the light and dark blue contours indicate the regions enclosing 68% and 95% of the posterior probability density. Comparing witth the black dashed line, indicating

https://doi.org/10.1017/S1743921322001144 Published online by Cambridge University Press

the 95% credible region of the prior distribution, illustrates the constraining power of high pulsar mass measurements for softer EoS.

2.2. *GW tidal deformability measurements*

One particularly interesting method to constrain the EoS is through GW measurements of the tidal deformability of neutron stars in merging binaries (Hinderer et al. (2010)). When a neutron star is sufficiently close to their compact binary companion, the tidal forces become strong enough to deform the neutron star. This results in additional energy from the binary being dissipated, on top of energy dissipated through GW emission, causing the binary to merge faster than if the components were black holes. The first ever detected binary neutron star merger, GW170817, allowed for upper limits on the dephasing of the signal due to tidal deformations, constraining the effective tidal deformability parameter to $\tilde{\Lambda} \sim\leqslant 800$ (Abbott et al. (2019)). The second binary neutron star merger, GW190425 (LIGO/Virgo Collaboration (2020)), was detected with a lower signal-to-noise ratio (S/N) of 12.9 and had a much higher total mass than GW170817. As a result, no significant constraints could be set on the tidal deformability of the stars. The upper right panel of 1 illustrates the constraints on the EoS from GW170817 and GW190425. Note that any constraints coming from GW190425 are only due to the relatively high measured masses, thus disfavouring some of the softest EoS. However, the upper limit on the tidal deformability from GW170817 disfavours some of the stiffest EoS, causing the overall posterior distribution on the EoS from GW detections to favour lower radii than compared to the posterior distributions from *NICER* (see subsection below).

2.3. *A NICER view on PSR J0030+0451 and PSR J0740+6620*

NICER , a soft X-ray instrument installed on board of the textitInternational Space Station in 2017, constrains the mass and radius of pulsars through a technique called pulse profile modeling. This technique uses general and special relativistic effects on the photons emitted by hot regions on the surface of fast-spinning pulsars, such as light-bending, Doppler boosting and abberation. Because these effects depend on the spacetime surrounding the neutron star, as well as the velocity of the emitting regions on the surface, we can infer information on the mass and radius of the star, given the spin of the star and a model for the surface emission (see, e.g., Watts et al. (2016) for a review). *NICER* is specifically applying pulse profile modeling to rotationally-powered millisecond pulsars, for which the high spin ensures that the relativistic effects are strong enough to be measured and the spin periods are extremely stable over long periods of time. The emitting regions for rotationally-powered millisecond pulsars are thought to be generated through a return current of positrons heating the surface at the polar caps, but the shape and location for these is highly uncertain (see, e.g., Gralla et al. (2017)).

In 2019, *NICER* inferred for the first time the mass and radius of a pulsar, PSR J0030+0451, reporting a mass of $M = 1.34^{+0.15}_{-0.16}$ $\mathrm{M}_{\odot}$ and a radius of $R_{eq} = 12.71^{+1.14}_{-1.19}$ km (Miller et al. (2019), Riley et al. (2019)) (see Figure 2). The relatively low pulsar mass and broad posterior support in radius resulted only in loose constraints on the EoS (see, e.g., Raaijmakers et al. (2019)).

In 2021, *NICER* published the mass and radius of a second pulsar, PSR J0740+6620 (Miller et al. (2021), Riley et al. (2021)). For this pulsar, an independent mass measurement exists from radio timing, which has been used as a prior in the *NICER* analysis. Even though the mass of the pulsar is much higher, $M = 2.072^{+0.067}_{-0.066}$ $\mathrm{M}_{\odot}$, the radius

https://doi.org/10.1017/S1743921322001144 Published online by Cambridge University Press

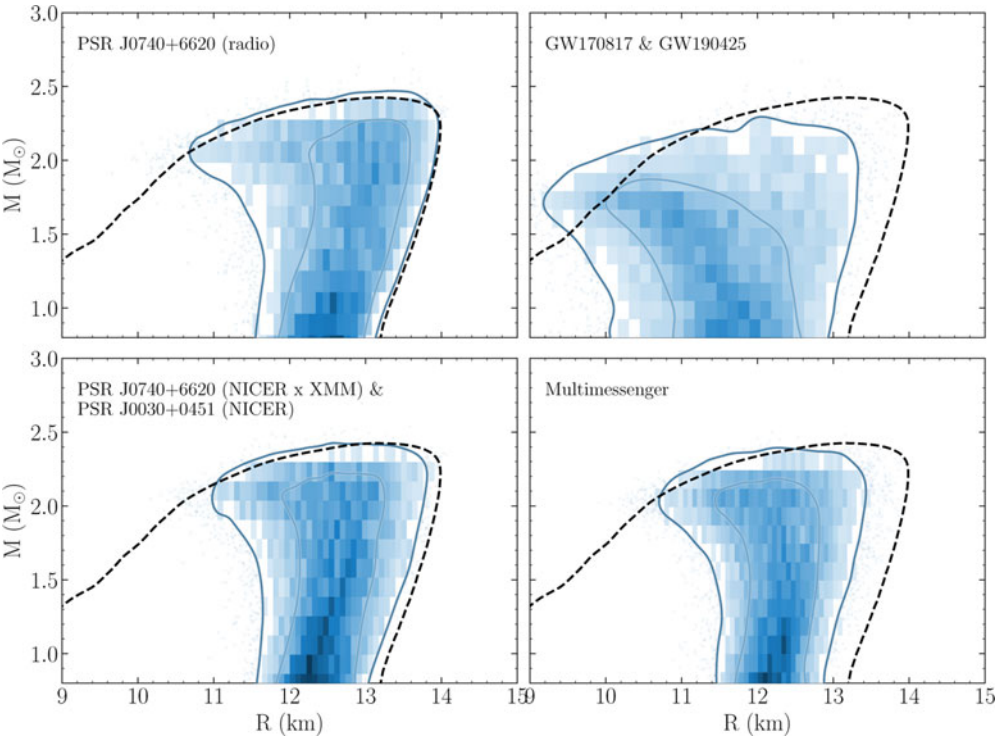

Figure 1. EoS constraints from multimessenger sources, when parameterizing the EoS with a piecewise-polytropic model. In each panel the black dashed line indicates the 95% credible region for the prior of our model, while the light and dark blue contours show the 68% and 95% credible regions of the posterior distribution of EoS (also shown as a two-dimensional histogram). From the upper left to the lower right panel the posterior distribution is inferred using a radio mass measurement of PSR J0740+6620, the gravitational wave measurements of GW170817 and GW190425, the *NICER* mass and radius measurements of PSR J0740+6620 and PSR J0030+0451, and using all of the previous combined.

is remarkably similar to PSR J0030+0451: $R_{eq} = 12.39^{+1.30}_{-0.98}$ km (see Figure 2), which disfavours EoS models with strong phase transitions (see, e.g., Legred et al. (2021)).

The impact of the measurements by *NICER* on the EoS is shown in the lower left panel of Figure 1 (see also Raaijmakers et al. (2021)). Comparing to the constraints from only including the mass of PSR J0740+66210 (upper left panel) illustrates the similarity in posterior distributions, a result of the *NICER* measurements favouring EoS that already had the most posterior support from including high mass pulsars and low-density nuclear calculations. In the lower right panel I show the posterior distribution on the EoS when combining all three other panels, resulting in the radius of a 1.4 $M_\odot$ neutron star to be constrained to $R_{eq} = 12.33^{+0.76}_{-0.81}$ km from multimessenger observations.

3. Multimessenger Analyses of Black Hole - Neutron Star Mergers

The first ever detection of a GW signal from a BNS merger, GW170817, was accompanied by a slew of observations of the associated EM counterparts across the frequency spectrum. These observations enabled additional information to be gained on, e.g., the Hubble constant (see, e.g., Abbott et al. (2017)), and the equation of state of dense matter (e.g., Raaijmakers et al. (2020)). The next big discovery in GW astrophysics would be a BHNS merger with an identified EM counterpart. During the third observing run of the LIGO/Virgo detectors two confident BHNS mergers were detected: GW200105 and

https://doi.org/10.1017/S1743921322001144 Published online by Cambridge University Press

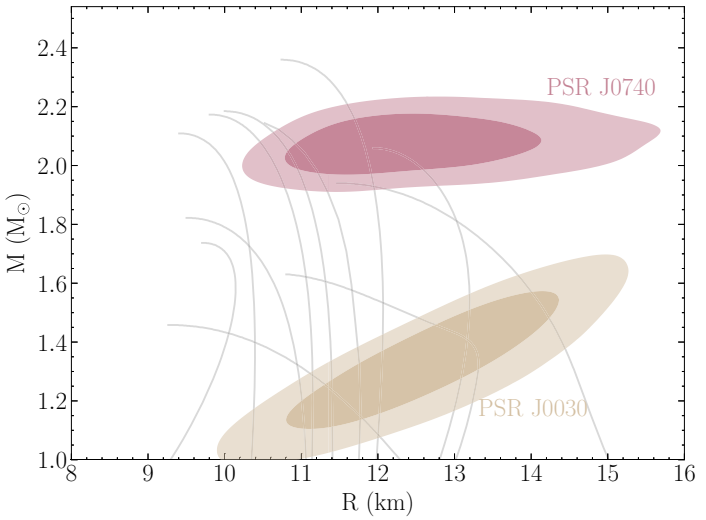

Figure 2. Mass and radius measurements of the first two pulsars analyzed by *NICER* , PSR J0030+0451 and PSR J0740+6620. The light and dark shaded regions bound 68% and 95% of the posterior probability density, and the grey lines indicate a variety of theoretical EoS models.

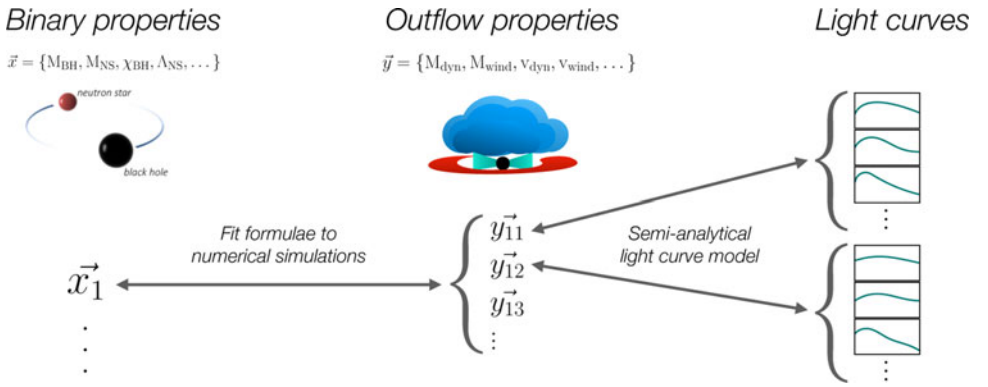

Figure 3. A schematic of the coupling between binary properties, here a BHNS system, the outflow properties of the ejected material and the kilonova light curves. In this model, a set of analytical formulae are fitted to a large array of numerical merger simulations, to map between the initial binary properties and the outflow properties (Krüger & Foucart (2020)). To obtain kilonova light curves from a set of outflow properties the semi-analytical light curve model by Hotokezaka & Nakar (2020) is used.

GW200115 (Abbott et al. (2021)). However, despite significant follow-up efforts, no EM counterparts were discovered (Anand et al. (2021)), which is not surprising given the relatively large mass ratios of the two systems (Zhu et al. (2021)).

3.1. *From Binary Properties to Kilonova Light Curves*

In the context of constraining the dense matter EoS, the kilonova accompanying both BNS and BHNS mergers is particularly interesting. Powered by the radio-active decay of heavey elements that are formed in the extremely neutron-rich material ejected during and after the merger, the peak and shape of the kilonova light curves in UVOIR photometric bands depend sensitively on the mass, velocity and opacity of the merger ejecta. These outflow properties are, in turn, directly coupled to the binary parameters such as

https://doi.org/10.1017/S1743921322001144 Published online by Cambridge University Press

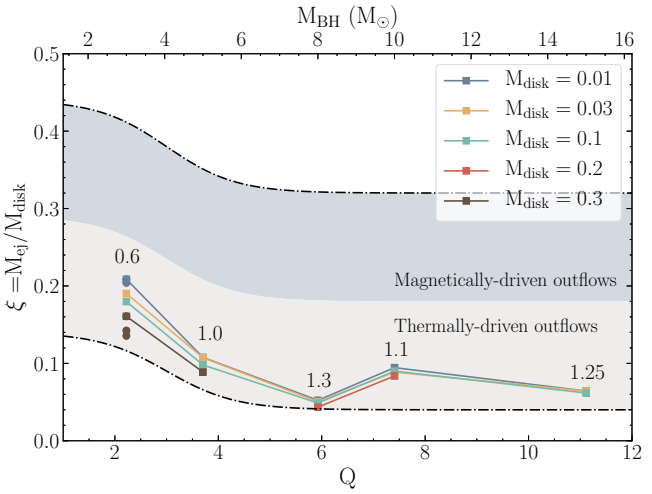

Figure 4. The uncertainty band of the fraction of the accretion disk that is eventually ejected, as a function of the mass ratio Q, as used in the framework of Raaijmakers et al. (2021). The data points correspond to viscous hydrodynamical simulations performed in Fernández et al. (2020), that are used to model the thermally-driven outflows in the disk. Based on the few available GRMHD simulations of the accretion disk, an additional 20% uncertainty is added to capture the magnetically-driven outflows.

the mass ratio and tidal deformability of the stars. A schematic of how we modeled the coupling between binary properties and kilonova light curves in Raaijmakers et al. (2021) is shown in Figure 3. To map the properties of an initial binary system to properties of the outflows during and after the merger, we used analytical formulae fitted to numerical merger simulations (see Krüger & Foucart (2020)). Due to both the uncertainty in the numerical merger simulations, from, e.g., incomplete input physics, and the uncertainty in the analytical fit, a single set of binary properties can predict multiple sets of outflow properties in our model. Similarly, uncertainty in the light curve modelling results in a range of possible light curves for a single set of outflow properties. In our framework we use a spherically symmetric, semi-analytical model to compute the bolometric light curve published by Hotokezaka & Nakar (2020), based on the work by Li & Paczyinski (1998).

The outflows in a BHNS merger can be further divided into different ejecta components. The first component, called the dynamical ejecta, comprises of material of the neutron star that becomes unbound after the star disrupts due to the extreme tidal forces (see, e.g., Foucart et al. (2017)). This generally corresponds to high-velocity, extremely neutron rich material, leading to emission peaking in the near-infrared (e.g., Kawaguchi et al. (2020)). The second component, called the disk ejecta, originates from the accretion disk that forms around the remnant BH after the merger. Based on its velocity, one can further divide the disk ejecta in two subcomponents. The slower, thermally-driven ejecta is caused by energy dissipation due to angular momentum transport. This subcomponent can be modeled relatively well with viscous hydrodynamical simulations, such as in Fernández et al. (2020). A faster, magnetically-driven component is seen in general-relativistic magnetohydrodynamic (GRMHD) simulations (see, e.g., Siegel & Metzger (2017); Fernández et al. (2019); De & Siegel (2021)). Due to the large computational cost of simulating merger outflows, especially in GRMHD, the fraction of the accretion disk that ultimately gets ejected is still one of the largest uncertainties in coupling the binary properties to kilonova light curves. Figure 4 shows the uncertainty band of this fraction as a function of the mass ratio of the system. The data points are from the

https://doi.org/10.1017/S1743921322001144 Published online by Cambridge University Press

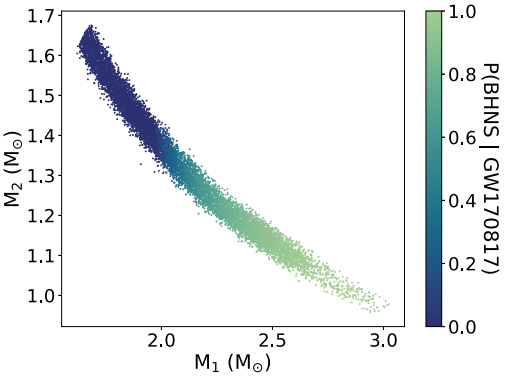

Figure 5. The component source masses of GW190425 (LIGO/Virgo Collaboration (2020)), color-coded by the probability of the system being a BHNS merger. The probability is calculated based on the maximum mass of neutron stars, given by the constraints on the EoS derived from GW170817.

viscous hydrodynamical simulations performed in Fernández et al. (2020), while for the magnetically-driven outflows an additional uncertainty of 20% is estimated.

3.2. *Joint Parameter Estimation on a GW190425-like Merger*

In Raaijmakers et al. (2021), we investigated additional constraints from joint parameter estimation of a GW signal and the kilonova lightcurves, taking GW190425 as a case study (LIGO/Virgo Collaboration (2020)), for which no EM counterpart was detected. It is interesting however, given the low S/N of the GW signal (12.9), what the potential is for constraining binary properties when a kilonova is detected. We will assume here that GW190425 originated from a BHNS merger: considering the component masses of GW190425 without assumptions on the spin magnitude, there is a non-negligible chance that GW190425 was a BHNS merger. This is illustrated in Figure 5, where the posterior samples in component source masses are plotted, color-coded by the probability of GW190425 being a BHNS merger given the constraints on the EoS from GW170817.

Taking all the uncertainties into account that are described above, we performed parameter estimation on a simulated GW190425-like GW signal and mock EM data in the g- and r-band (with an uncertainty in magnitude of $\sigma_{EM} = 0.2$). Figure 6 shows the constraints on a few key binary parameters, the mass ratio Q, the tidal deformability of the neutron star Λ_2 and the spin of the black hole χ_1. Most notable is the constraining power of the kilonova data on the tidal deformability of the neutron star, due to the sensitive dependence of the ejecta mass on Λ_2.

4. Outlook

The next few years will potentially see significant improvements of our understanding of the EoS of dense matter from astrophysical observations. Firstly, *NICER* is expected to deliver multiple mass-radius measurements in the near-future. Two of these, the 1.4 $M_\odot$ pulsar PSR J0437-4715 and the ~ 1.9 $M_\odot$ pulsar PSR J1614−2230, are particularly interesting because of their independent mass measurements. The third source, pulsar PSR J1231−1411, has no independently known constraint on the mass. Furthermore, updates on the previously published results on PSR J0030+0451 and PSR J0740+6620 are also expected.

Secondly, the next observing run of the LIGO/Virgo/KAGRA detectors is scheduled to commence at the end of 2022, potentially increasing the population of observed

https://doi.org/10.1017/S1743921322001144 Published online by Cambridge University Press

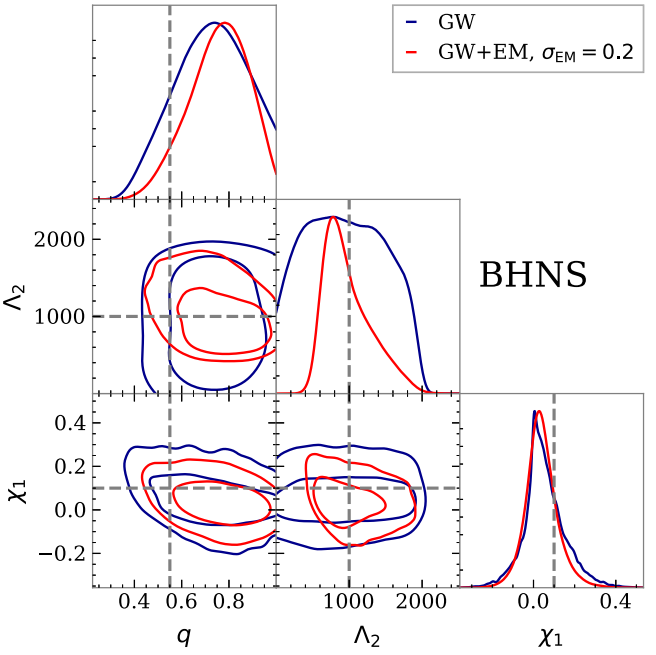

Figure 6. Posterior distributions on a few key quantities describing the binary system. The contours in the 2D plots bound 68% and 95% of the posterior density. Most notable is the additional constraint on the tidal deformability of the neutron star when jointly analyzing the GW data and kilonova light curves.

binary mergers involving a neutron star, and thus tidal deformability measurements. Additionally, higher-accuracy EM data and larger number of detected EM counterparts are possible due to current and near-future telescopes such as the Vera Rubin Observatory (Ivezić et al. (2019)), the Zwicky Transient Facility (Dekany et al. (2020)), BlackGEM (Bloemen et al. (2016)) and GOTO (Gompertz et al. (2020)).

Jointly analyzing the rich data available in the near-future from *NICER* and multimessenger GW events will allow us to constrain the EoS of neutron stars to unprecedented accuracy, and as a result learn more about the fundamental forces that govern dense matter physics.

References

Abbott, B. P., Abbott, R., Abbott, T. D., et al. 2017, *Phys. Rev. Lett.*, 119, 161101
Abbott, B. P., Abbott, R., Abbott, T. D., et al. 2017, Nature, 551, 85
Abbott, B. P., Abbott, R., Abbott, T. D., et al. 2018, *Phys. Rev. Lett.*, 121, 161101
Abbott, B. P., Abbott, R., Abbott, T. D., et al. 2019, Physical Review X, 9, 031040
Abbott, B. P., Abbott, R., Abbott, T. D., et al. 2020, *ApJ* (Letters), 892, L3
Abbott, R., Abbott, T. D., Abraham, S., et al. 2021, *ApJ* (Letters), 915, L5
Anand, S., Coughlin, M. W., Kasliwal, M. M., et al. 2021, Nature Astronomy, 5, 46
Baym, G., Hatsuda, T., Kojo, T., et al. 2018, Reports on Progress in Physics, 81, 056902.
Bloemen, S., Groot, P., Woudt, P., et al. 2016, *Proceedings of the SPIE*, 9906, 990664
Capano, C. D., Tews, I., Brown, S. M., et al. 2020, Nature Astronomy, 4, 625
Cromartie, H. T., Fonseca, E., Ransom, S. M., et al. 2020, Nature Astronomy, 4, 72
De, S. & Siegel, D. M. 2021, *ApJ*, 921, 94
Dekany, R., Smith, R. M., Riddle, R., et al. 2020, *Publications of the Astronomical Society of the Pacific*, 132, 038001
Essick, R., Landry, P., & Holz, D. E. 2020, *Phys. Rev. D*, 101, 063007

https://doi.org/10.1017/S1743921322001144 Published online by Cambridge University Press

Fernández, R., Tchekhovskoy, A., Quataert, E., et al. 2019, *MNRAS*, 482, 3373
Fernández, R., Foucart, F., & Lippuner, J. 2020, *MNRAS*, 497, 3221
Fonseca, E., Cromartie, H. T., Pennucci, T. T., et al. 2021, *ApJ* (Letters), 915, L12
Foucart, F., Desai, D., Brege, W., et al. 2017, Classical and Quantum Gravity, 34, 044002
Gompertz, B. P., Cutter, R., Steeghs, D., et al. 2020, *MNRAS*, 497, 726
Gralla, S. E., Lupsasca, A., & Philippov, A. 2017, *ApJ*, 851, 137
Greif, S. K., Raaijmakers, G., Hebeler, K., et al. 2019, *MNRAS*, 485, 5363
Hebeler, K., Lattimer, J. M., Pethick, C. J., et al. 2013, *ApJ*, 773, 11
Hinderer, T., Lackey, B. D., Lang, R. N., et al. 2010, *Phys. Rev. D*, 81, 123016
Hotokezaka, K. & Nakar, E. 2020, *ApJ*, 891, 152
Ivezić, Ž., Kahn, S. M., Tyson, J. A., et al. 2019, *ApJ*, 873, 111
Kawaguchi, K., Shibata, M., & Tanaka, M. 2020, *ApJ*, 889, 171
Krüger, C. J. & Foucart, F. 2020, *Phys. Rev. D*, 101, 103002
Landry, P. & Essick, R. 2019, *Phys. Rev. D*, 99, 084049
Legred, I., Chatziioannou, K., Essick, R., et al. 2021, *Phys. Rev. D*, 104, 063003
Li, L.-X. & Paczyński, B. 1998, *ApJ* (Letters), 507, L59
Lindblom, L. 2010, *Phys. Rev. D*, 82, 103011
Metzger, B. D. 2019, Living Reviews in Relativity, 23, 1
Miller, M. C., Lamb, F. K., Dittmann, A. J., et al. 2019, *ApJ* (Letters), 887, L24
Miller, M. C., Lamb, F. K., Dittmann, A. J., et al. 2021, *ApJ* (Letters), 918, L28
Pang, P. T. H., Tews, I., Coughlin, M. W., et al. 2021, *ApJ*, 922, 1
Raaijmakers, G., Riley, T. E., Watts, A. L., et al. 2019, *ApJ* (Letters), 887, L22
Raaijmakers, G., Greif, S. K., Riley, T. E., et al. 2020, *ApJ* (Letters), 893, L21
Raaijmakers, G., Greif, S. K., Hebeler, K., et al. 2021, *ApJ* (Letters), 918, L29
Raaijmakers, G., Nissanke, S., Foucart, F., et al. 2021, *ApJ*, 922, 269
Read, J. S., Lackey, B. D., Owen, B. J., et al. 2009, *Phys. Rev. D*, 79, 124032
Riley, T. E., Watts, A. L., Bogdanov, S., et al. 2019, *ApJ* (Letters), 887, L21
Riley, T. E., Watts, A. L., Ray, P. S., et al. 2021, *ApJ* (Letters), 918, L27
Siegel, D. M. & Metzger, B. D. 2017, *Phys. Rev. Lett.*, 119, 231102
Watts, A. L., Andersson, N., Chakrabarty, D., et al. 2016, Reviews of Modern Physics, 88, 021001
Zhu, J.-P., Wu, S., Yang, Y.-P., et al. 2021, *ApJ*, 921, 156

https://doi.org/10.1017/S1743921322001144 Published online by Cambridge University Press